A Phase-Based Iris Recognition Algorithm

Kazuyuki Miyazawa[1], Koichi Ito[1], Takafumi Aoki[1], Koji Kobayashi[2], and Hiroshi Nakajima[2]

[1] Graduate School of Information Sciences, Tohoku University, Sendai 980–8579, Japan
miyazawa@aoki.ecei.tohoku.ac.jp
[2] Yamatake Corporation, Isehara 259–1195, Japan

Abstract. This paper presents an efficient algorithm for iris recognition using phase-based image matching. The use of phase components in two-dimensional discrete Fourier transforms of iris images makes possible to achieve highly robust iris recognition with a simple matching algorithm. Experimental evaluation using the CASIA iris image database (ver. 1.0 and ver. 2.0) clearly demonstrates an efficient performance of the proposed algorithm.

1 Introduction

Biometric authentication has been receiving extensive attention over the past decade with increasing demands in automated personal identification. Among many biometrics techniques, iris recognition is one of the most promising approaches due to its high reliability for personal identification [1–8].

A major approach for iris recognition today is to generate feature vectors corresponding to individual iris images and to perform iris matching based on some distance metrics [3–6]. Most of the commercial iris recognition systems implement a famous algorithm using iriscodes proposed by Daugman [3]. One of the difficult problems in feature-based iris recognition is that the matching performance is significantly influenced by many parameters in feature extraction process (eg., spatial position, orientation, center frequencies and size parameters for 2D Gabor filter kernel), which may vary depending on environmental factors of iris image acquisition. Given a set of test iris images, extensive parameter optimization is required to achieve higher recognition rate.

Addressing the above problem, as one of the algorithms which compares iris images directly without encoding [7, 8], this paper presents an efficient algorithm using phase-based image matching – an image matching technique using only the phase components in 2D DFTs (Two-Dimensional Discrete Fourier Transforms) of given images. The technique has been successfully applied to high-accuracy image registration tasks for computer vision applications [9–11], where estimation of sub-pixel image translation is a major concern. In our previous work [12], on the other hand, we have proposed an efficient fingerprint recognition algorithm using phase-based image matching, and have developed commercial fingerprint verification units [13]. In this paper, we demonstrate that the

D. Zhang and A.K. Jain (Eds.): ICB 2006, LNCS 3832, pp. 356–365, 2005.

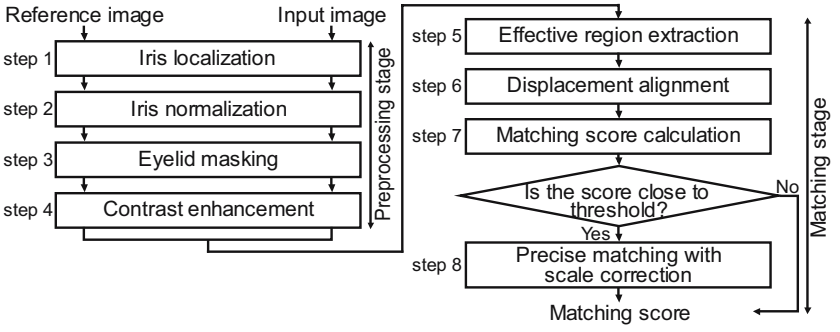

Fig. 1. Flow diagram of the proposed algorithm

same technique is also highly effective for iris recognition. The use of Fourier phase information of iris images makes possible to achieve highly robust iris recognition in a unified fashion with a simple matching algorithm. Experimental performance evaluation using the CASIA iris image database ver. 1.0 and ver. 2.0 [14] clearly demonstrates an efficient matching performance of the proposed algorithm.

Figure 1 shows the overview of the proposed algorithm. The algorithm consists of two stages: (i) preprocessing stage (step 1 – step 4) and (ii) matching stage (step 5 – step 8). Section 2 describes the image preprocessing algorithm (stage (i)). Section 3 presents the iris matching algorithm (stage (ii)). Section 4 discusses experimental evaluation.

2 Preprocessing

An iris image contains some irrelevant parts (eg., eyelid, sclera, pupil, etc.). Also, even for the iris of the same eye, its size may vary depending on camera-to-eye distance as well as light brightness. Therefore, before matching, the original image needs to be preprocessed to localize and normalize the iris.

2.1 Iris Localization

This step is to detect the inner (iris/pupil) boundary and the outer (iris/sclera) boundary in the original image $f_{org}(m_1, m_2)$ shown in Figure 2(a). Through a set of experiments, we decided to use an ellipse as a model of the inner boundary. Let (l_1, l_2) be the lengths of the two principal axes of the ellipse, (c_1, c_2) be its center, and θ be the rotation angle. We can find the optimal estimate $(l_1, l_2, c_1, c_2, \theta)$ for the inner boundary by maximizing the following absolute difference:

$$|S(l_1 + \Delta l_1, l_2 + \Delta l_2, c_1, c_2, \theta) - S(l_1, l_2, c_1, c_2, \theta)|\,. \tag{1}$$

Here, Δl_1 and Δl_2 are small constants, and S denotes the N-point contour summation of pixel values along the ellipse and is defined as

$$S(l_1, l_2, c_1, c_2, \theta) = \sum_{n=0}^{N-1} f_{org}(p_1(n), p_2(n)), \tag{2}$$

where $p_1(n) = l_1 \cos\theta \cdot \cos(\frac{2\pi}{N}n) - l_2 \sin\theta \cdot \sin(\frac{2\pi}{N}n) + c_1$ and $p_2(n) = l_1 \sin\theta \cdot \cos(\frac{2\pi}{N}n) + l_2 \cos\theta \cdot \sin(\frac{2\pi}{N}n) + c_2$. Thus, we will detect the inner boundary as the ellipse on the image for which there will be sudden change in luminance summed around its perimeter. In order to reduce computation time, the parameter set $(l_1, l_2, c_1, c_2, \theta)$ can be simplified depending on iris images. For example, in our experiments using the CASIA iris image database ver. 1.0 and ver. 2.0, assuming $\theta = 0$ causes no degradation on its performance. The outer boundary, on the other hand, is detected in a similar manner, with the path of contour summation changed from ellipse to circle (i.e., $l_1 = l_2$).

2.2 Iris Normalization and Eyelid Masking

Next step is to normalize iris to compensate for the deformations in iris texture. We unwrap the iris region to a normalized (scale corrected) rectangular block with a fixed size (256×128 pixels). In order to remove the iris region occluded by the upper eyelid and eyelashes, we use only the lower half (Figure 2(a)) and apply a polar coordinate transformation (with its origin at the center of pupil) to obtain the normalized image shown in Figure 2(b), where n_1 axis corresponds to the angle of polar coordinate system and n_2 axis corresponds to the radius.

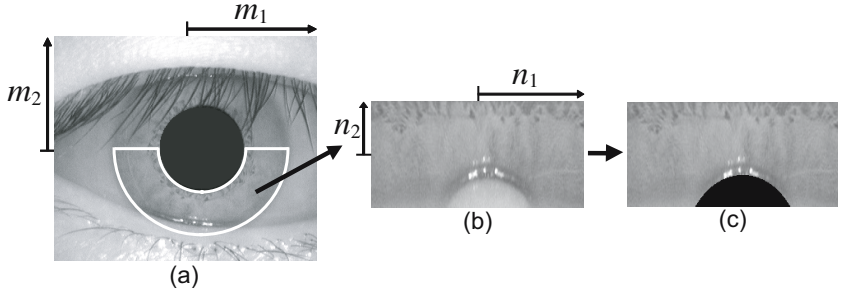

Fig. 2. Iris image: (a) original image $f_{org}(m_1, m_2)$, (b) normalized image, and (c) normalized image with eyelid masking $\tilde{f}(n_1, n_2)$

In general, the eyelid boundary can be modeled as an elliptical contour. Hence the same method for detecting the inner boundary can be applied to eyelid detection. The detected eyelid region is masked as shown in Figure 2(c).

2.3 Contrast Enhancement

In some situation, the normalized iris image has low contrast. Typical examples of such iris images are found in the CASIA iris image database ver. 2.0. In such a case, we improve the contrast by using local histogram equalization technique [4]. Figure 3 shows an example of contrast enhancement.

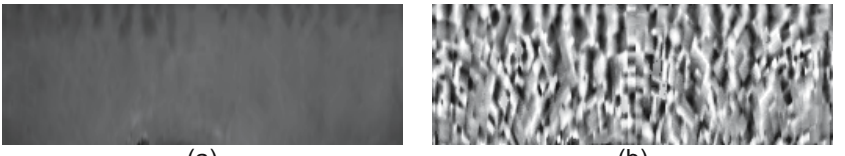

Fig. 3. Contrast enhancement: (a) normalized iris image, and (b) enhanced image

3 Matching

In this section, we describe the detailed process of effective region extraction (section 3.2), image alignment (section 3.3) and matching score calculation (section 3.4 and section 3.5). The key idea in this paper is to use phase-based image matching for image alignment and matching score calculation. Before discussing the algorithm, section 3.1 introduces the principle of phase-based image matching using the Phase-Only Correlation (POC) function [10–12].

3.1 Fundamentals of Phase-Based Image Matching

Consider two $N_1 \times N_2$ images, $f(n_1, n_2)$ and $g(n_1, n_2)$, where we assume that the index ranges are $n_1 = -M_1 \cdots M_1$ $(M_1 > 0)$ and $n_2 = -M_2 \cdots M_2$ $(M_2 > 0)$ for mathematical simplicity, and hence $N_1 = 2M_1 + 1$ and $N_2 = 2M_2 + 1$. Let $F(k_1, k_2)$ and $G(k_1, k_2)$ denote the 2D DFTs of the two images. $F(k_1, k_2)$ is given by

$$F(k_1, k_2) = \sum_{n_1=-M_1}^{M_1} \sum_{n_2=-M_2}^{M_2} f(n_1, n_2) W_{N_1}^{k_1 n_1} W_{N_2}^{k_2 n_2} = A_F(k_1, k_2) e^{j\theta_F(k_1, k_2)}, \quad (3)$$

where $k_1 = -M_1 \cdots M_1$, $k_2 = -M_2 \cdots M_2$, $W_{N_1} = e^{-j\frac{2\pi}{N_1}}$, and $W_{N_2} = e^{-j\frac{2\pi}{N_2}}$. $A_F(k_1, k_2)$ is amplitude and $\theta_F(k_1, k_2)$ is phase. $G(k_1, k_2)$ is defined in the same way. The cross-phase spectrum $R_{FG}(k_1, k_2)$ between $F(k_1, k_2)$ and $G(k_1, k_2)$ is given by

$$R_{FG}(k_1, k_2) = \frac{F(k_1, k_2)\overline{G(k_1, k_2)}}{|F(k_1, k_2)\overline{G(k_1, k_2)}|} = e^{j\theta(k_1, k_2)}, \quad (4)$$

where $\overline{G(k_1, k_2)}$ is the complex conjugate of $G(k_1, k_2)$ and $\theta(k_1, k_2)$ denotes the phase difference $\theta_F(k_1, k_2) - \theta_G(k_1, k_2)$. The POC function $r_{fg}(n_1, n_2)$ is the 2D inverse DFT of $R_{FG}(k_1, k_2)$ and is given by

$$r_{fg}(n_1, n_2) = \frac{1}{N_1 N_2} \sum_{k_1=-M_1}^{M_1} \sum_{k_2=-M_2}^{M_2} R_{FG}(k_1, k_2) W_{N_1}^{-k_1 n_1} W_{N_2}^{-k_2 n_2}. \quad (5)$$

When two images are similar, their POC function gives a distinct sharp peak. When two images are not similar, the peak value drops significantly. The height

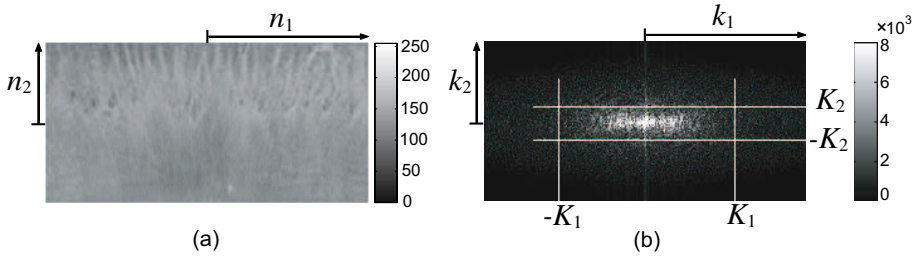

Fig. 4. Normalized iris image in (a) spatial domain, and in (b) frequency domain (amplitude spectrum)

of the peak can be used as a similarity measure for image matching, and the location of the peak shows the translational displacement between the two images.

In our previous work on fingerprint recognition [12], we have proposed the idea of BLPOC (Band-Limited Phase-Only Correlation) function for efficient matching of fingerprints considering the inherent frequency components of fingerprint images. Through a set of experiments, we have found that the same idea is also very effective for iris recognition. Our observation shows that (i) the 2D DFT of a normalized iris image sometimes includes meaningless phase components in high frequency domain, and that (ii) the effective frequency band of the normalized iris image is wider in k_1 direction than in k_2 direction as illustrated in Figure 4. The original POC function $r_{fg}(n_1, n_2)$ emphasizes the high frequency components, which may have less reliability. We observe that this reduces the height of the correlation peak significantly even if the given two iris images are captured from the same eye. On the other hand, BLPOC function allows us to evaluate the similarity using the inherent frequency band within iris textures.

Assume that the ranges of the inherent frequency band are given by $k_1 = -K_1 \cdots K_1$ and $k_2 = -K_2 \cdots K_2$, where $0 \leq K_1 \leq M_1$ and $0 \leq K_2 \leq M_2$. Thus, the effective size of frequency spectrum is given by $L_1 = 2K_1 + 1$ and $L_2 = 2K_2 + 1$. The BLPOC function is given by

$$r_{fg}^{K_1 K_2}(n_1, n_2) = \frac{1}{L_1 L_2} \sum_{k_1=-K_1}^{K_1} \sum_{k_2=-K_2}^{K_2} R_{FG}(k_1, k_2) W_{L_1}^{-k_1 n_1} W_{L_2}^{-k_2 n_2}, \qquad (6)$$

where $n_1 = -K_1 \cdots K_1$ and $n_2 = -K_2 \cdots K_2$. Note that the maximum value of the correlation peak of the BLPOC function is always normalized to 1 and does not depend on L_1 and L_2. Also, the translational displacement between the two images can be estimated by the correlation peak position.

In our algorithm, K_1/M_1 and K_2/M_2 are major control parameters, since these parameters reflect the quality of iris images. In our experiments, $K_1/M_1 = 0.6$ and $K_2/M_2 = 0.2$ are used for the CASIA iris image database ver. 1.0, and $K_1/M_1 = 0.55$ and $K_2/M_2 = 0.2$ are used for the CASIA iris image database ver. 2.0. It is interesting to note that iris images in both databases have effective frequency band of only 20% in k_2 direction (radius direction of iris).

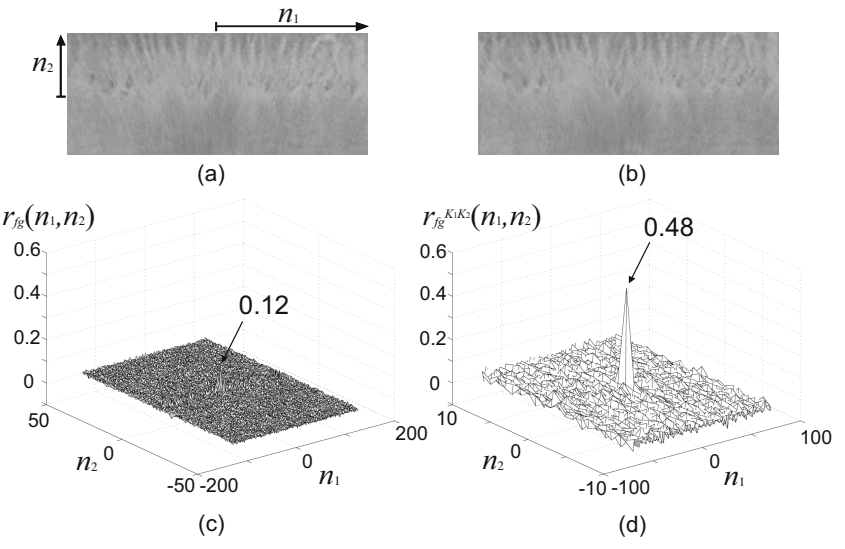

Fig. 5. Example of genuine matching using the original POC function and the BLPOC function: (a) iris image $f(n_1, n_2)$, (b) iris image $g(n_1, n_2)$, (c) original POC function $r_{fg}(n_1, n_2)$, and (d) BLPOC function $r_{fg}^{K_1 K_2}(n_1, n_2)$ ($K_1/M_1 = 0.6$, $K_2/M_2 = 0.2$).

Figure 5 shows an example of genuine matching, where the figure compares the original POC function r_{fg} and the BLPOC function $r_{fg}^{K_1 K_2}$ ($K_1/M_1 = 0.6$ and $K_2/M_2 = 0.2$). The BLPOC function provides a higher correlation peak than that of the original POC function. Thus, the BLPOC function exhibits a much higher discrimination capability than the original POC function.

In the following, we explain the step 5 – step 8 in Figure 1. The above mentioned BLPOC function is used in step 6 (displacement alignment), step 7 (matching score calculation) and step 8 (precise matching with scale correction).

3.2 Effective Region Extraction

Given a pair of normalized iris images $\tilde{f}(n_1, n_2)$ and $\tilde{g}(n_1, n_2)$ to be compared, the purpose of this process is to extract effective regions of the same size from the two images, as illustrated in Figure 6(a). Let the size of two images $\tilde{f}(n_1, n_2)$ and $\tilde{g}(n_1, n_2)$ be $\tilde{N}_1 \times \tilde{N}_2$, and let the widths of irrelevant regions in $\tilde{f}(n_1, n_2)$ and $\tilde{g}(n_1, n_2)$ be $w_{\tilde{f}}$ and $w_{\tilde{g}}$, respectively. We obtain $f(n_1, n_2)$ and $g(n_1, n_2)$ by extracting effective regions of size $\tilde{N}_1 \times \{\tilde{N}_2 - \max(w_{\tilde{f}}, w_{\tilde{g}})\}$ through eliminating irrelevant regions such as masked eyelid and specular reflections.

On the other hand, a problem occurs when the extracted effective region becomes too small to perform image matching. In this case, by changing the parameter w, we extract multiple effective sub-regions from each iris image as illustrated in Figure 6(b). In our experiments, we extract at most 6 sub-regions from a single iris image by changing the parameter w as 55, 75 and 95 pixels.

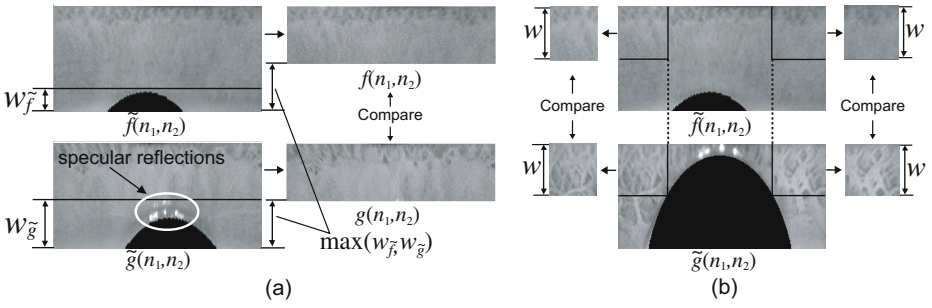

Fig. 6. Effective region extraction: (a) normal case, and (b) case when multiple sub-regions should be extracted

3.3 Displacement Alignment

This step is to align the translational displacement τ_1 and τ_2 between the extracted images $f(n_1, n_2)$ and $g(n_1, n_2)$. Rotation of the camera, head tilt and rotation of the eye within the eye socket may cause the displacements in normalized images (due to the polar coordinate transformation). The displacement parameters (τ_1, τ_2) can be estimated from the peak location of the BLPOC function $r_{fg}^{K_1 K_2}(n_1, n_2)$. The obtained parameters are used to align the images.

3.4 Matching Score Calculation

In this step, we calculate the BLPOC function $r_{fg}^{K_1 K_2}(n_1, n_2)$ between the aligned images $f(n_1, n_2)$ and $g(n_1, n_2)$, and evaluate the matching score. In the case of genuine matching, if the displacement between the two images is aligned, the correlation peak of the BLPOC function should appear at the origin $(n_1, n_2) = (0, 0)$. So, we calculate the matching score between the two images as the maximum peak value of the BLPOC function within the $r \times r$ window centered at the origin, where we choose $r = 11$ in our experiments. When multiple sub-regions are extracted at the "effective region extraction" process, the matching score is calculated by taking an average of matching scores for the sub-regions.

3.5 Precise Matching with Scale Correction

For some iris images, errors take place in estimating the center coordinates of the iris and the pupil in the preprocessing. In such a case, slight scaling of the normalized images may occur. And the matching score drops to a lower value even if the given two iris images are captured from the same eye. Then, if the matching score is close to threshold value to separate genuine and impostor, we generate a set of slightly scaled images (scaled in the n_1 direction), and calculate matching scores for the generated images. We select their maximum value as the final matching score.

4 Experiments and Discussions

This section describes a set of experiments using the CASIA iris image database ver. 1.0 and ver. 2.0 [14] for evaluating matching performance.

- **CASIA iris image database ver. 1.0.** This database contains 756 eye images with 108 unique eyes and 7 different images of each unique eye. We first evaluate the genuine matching scores for all the possible combinations of genuine attempts; the number of attempts is ${}_7C_2 \times 108 = 2268$. Next, we evaluate the impostor matching scores for all the possible combinations of impostor attempts; the number of attempts is ${}_{108}C_2 \times 7^2 = 283122$.
- **CASIA iris image database ver. 2.0.** This database contains 1200 eye images with 60 unique eyes and 20 different images of each unique eye. We first evaluate the genuine matching scores for all the possible combinations of genuine attempts; the number of attempts is ${}_{20}C_2 \times 60 = 11400$. Next, we evaluate the impostor matching scores for ${}_{60}C_2 \times 4^2 = 28320$ impostor attempts, where we take 4 images for each eye and make all the possible combinations of impostor attempts.

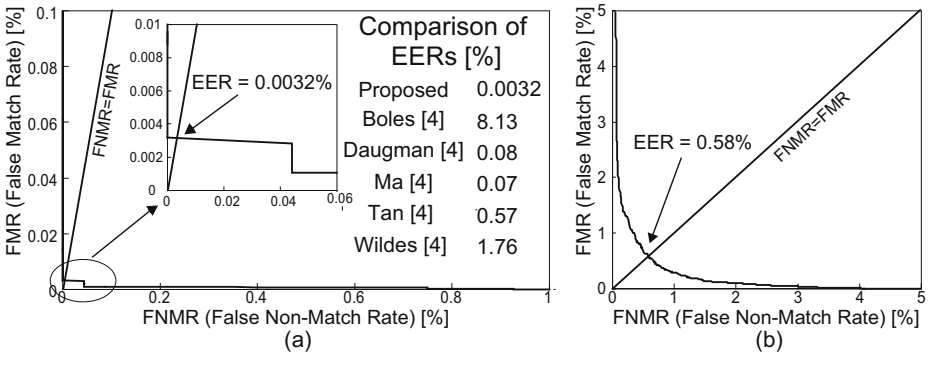

Fig. 7. ROC curve and EER: (a) CASIA iris image database ver. 1.0, and (b) ver. 2.0

Figure 7(a) shows the ROC (Receiver Operating Characteristic) curve of the proposed algorithm for the database ver. 1.0. The ROC curve illustrates FNMR (False Non-Match Rate) against FMR (False Match Rate) at different thresholds on the matching score. EER (Equal Error Rate) shown in the figure indicates the error rate where FNMR and FMR are equal. As is observed in the figure, the proposed algorithm exhibits very low EER (0.0032%). Some reported values of EER from [4] using the CASIA iris image database ver. 1.0 are shown in the same figure for reference. Note that the experimental condition in [4] is not the same as our case, because the complete database used in [4] is not available at CASIA [14] due to the limitations on usage rights of the iris images.

Figure 7(b) shows the ROC curve for the database ver. 2.0. The quality of the iris images in this database are poor, and it seems that the recognition task is difficult for most of the reported algorithms. Although we cannot find any reliable official report on recognition test for this database, we believe that our result (EER=0.58%) may be one of the best performance records that can be achieved at present for this kind of low-quality iris images. All in all, the above mentioned two experimental trials clearly demonstrate a potential possibility of phase-based image matching for creating an efficient iris recognition system.

5 Conclusion

The authors have already developed commercial fingerprint verification units [13] using phase-based image matching. In this paper, we have demonstrated that the same approach is also highly effective for iris recognition task. It can also be suggested that the proposed approach will be highly useful for multimodal biometric system having iris and fingerprint recognition capabilities.

Acknowledgment. Portions of the research in this paper use the CASIA iris image database ver 1.0 and ver 2.0 collected by Institute of Automation, Chinese Academy of Sciences.

References

1. Wayman, J., Jain, A., Maltoni, D., Maio, D.: Biometric Systems. Springer (2005)
2. Jain, A., Bolle, R., Pankanti, S.: Biometrics: Personal Identification in a Networked Society. Norwell, MA: Kluwer (1999)
3. Daugman, J.: High confidence visual recognition of persons by a test of statistical independence. IEEE Trans. Pattern Analy. Machine Intell. **15** (1993) 1148–1161
4. Ma, L., Tan, T., Wang, Y., Zhang, D.: Efficient iris recognition by characterizing key local variations. IEEE Trans. Image Processing **13** (2004) 739–750
5. Boles, W., Boashash, B.: A human identification technique using images of the iris and wavelet transform. IEEE Trans. Signal Processing **46** (1998) 1185–1188
6. Tisse, C., Martin, L., Torres, L., Robert, M.: Person identification technique using human iris recognition. Proc. Vision Interface (2002) 294–299
7. Wildes, R.: Iris recognition: An emerging biometric technology. Proc. IEEE **85** (1997) 1348–1363
8. Kumar, B., Xie, C., Thornton, J.: Iris verification using correlation filters. Proc. 4th Int. Conf. Audio- and Video-based Biometric Person Authentication (2003) 697–705
9. Kuglin, C.D., Hines, D.C.: The phase correlation image alignment method. Proc. Int. Conf. on Cybernetics and Society (1975) 163–165
10. Takita, K., Aoki, T., Sasaki, Y., Higuchi, T., Kobayashi, K.: High-accuracy subpixel image registration based on phase-only correlation. IEICE Trans. Fundamentals **E86-A** (2003) 1925–1934

11. Takita, K., Muquit, M.A., Aoki, T., Higuchi, T.: A sub-pixel correspondence search technique for computer vision applications. IEICE Trans. Fundamentals **E87-A** (2004) 1913–1923
12. Ito, K., Nakajima, H., Kobayashi, K., Aoki, T., Higuchi, T.: A fingerprint matching algorithm using phase-only correlation. IEICE Trans. Fundamentals **E87-A** (2004) 682–691
13. http://www.aoki.ecei.tohoku.ac.jp/poc/
14. http://www.sinobiometris.com